Prepared for submission to JINST

Laser Aided Plasma Diagnostic Conference
September 22-26, 2019
Whitefish, Montana, USA

Collective Thomson Scattering Diagnostic for Wendelstein 7-X at 175 GHz

D. Moseev,[a,1] H.P. Laqua,[a] T. Stange,[a] I. Abramovic,[a,b] S.K. Nielsen,[c] S. Äkäslompolo,[a] K. Avramidis,[d] H. Braune,[a] G. Gantenbein,[d] S. Illy,[d] J. Jelonnek,[d] J. Jin,[d] W. Kasparek,[e] L. Krier,[d] S.B. Korsholm,[c] C. Lechte,[e] A. Marek,[d] S. Marsen,[a] M. Nishiura,[f] I. Pagonakis,[d] M. Salewski,[c] J. Rasmussen,[c] A. Tancetti,[c] M. Thumm,[d] R.C. Wolf[a] and W7-X Team.

[a] *Max-Planck-Institut für Plasmaphysik, Greifswald, Germany*
[b] *Technical University of Eindhoven, Eindhoven, The Netherlands*
[c] *Technical University of Denmark, Kgs. Lyngby, Denmark*
[d] *Karlsruhe Institute of Technology, Karlsruhe, Germany*
[e] *Institute of Interfacial Process Engineering and Plasma Technology, University of Stuttgart, Stuttgart, Germany*
[f] *National Institute for Fusion Science, Toki, Japan*

E-mail: dmitry.moseev@ipp.mpg.de

Abstract: The Collective Thomson Scattering (CTS) diagnostic measures the scattering spectrum of incident radiation off collective fluctuations in plasmas. In Wendelstein 7-X (W7-X) the diagnostic uses a 140 GHz heating gyrotron as a source of the probing radiation. At this frequency, the CTS spectra are heavily affected by the electron cyclotron emission, and the microwave beam propagation is restricted at typical W7-X plasma parameters. The diagnostic was successfully commissioned in the last experimental campaign and demonstrated ion temperature measurements. However, the signal-to-noise ratio was too low for measuring other quantities such as the fast-ion velocity distribution function or the fuel ion ratio. Currently, the W7-X CTS diagnostic is undergoing an upgrade to a frequency of 175 GHz. This will increase the sensitivity of the diagnostic, since the noise due to electron cyclotron emission will be reduced, and it will relax the constraints on microwave beam propagation in W7-X. Here we present the salient features of the upgraded CTS system and discuss its prospects for both thermal-ion and fast-ion measurements.

[1] Corresponding author.

Contents

1 Introduction

Collective Thomson scattering (CTS) is based on scattering of probing radiation (most frequently microwaves) off collective fluctuations in the plasma. A CTS diagnostic is installed at the stellarator Wendelstein 7-X (W7-X) in order to measure the ion temperature. The diagnostic is installed at two different cross-sections of the stellarator, namely in the bean-shaped and triangular cross-sections. 140 GHz heating gyrotrons are used as a source of probing radiation [1]. Here eCTS, a java code integrated into the Bayesian analysis framework Minerva, has been developed and used for the analysis of experimental data [2–4]. The first experimental results on ion temperature measurements in the bean-shaped cross-section are reported in reference [1]. The results from the triangular cross-section of W7-X are currently being analyzed and prepared for publication.
Using heating gyrotrons as a source of probing radiation is not a usual diagnostic setup, and this has previously been done only at ASDEX Upgrade [5]. Typically, the probing frequency is chosen to minimize the electron cyclotron emission background, which allows measurements with good signal-to-noise ratio in reasonable integration times. In that case, the diagnostic can be used not only for measuring thermal-ion plasma properties (temperature, rotation velocity, isotope composition) [6–11], but also a projection of the fast-ion velocity distribution function [12–21]. The measurements of the diagnostic can further be used in tomographic reconstructions of the fast ion velocity distribution function [22–26]. More details on the diagnostic are found in the review [27].

2 140 GHz collective Thomson scattering diagnostic at Wendelstein 7-X

At Wendelstein 7-X, the CTS diagnostic uses the existing infrastructure of the electron cyclotron resonance heating (ECRH) facility [28–31]. The details of the diagnostic can be found in reference [1], so here we focus on the implications of using heating gyrotrons. The ECRH plant is presently equipped with 10 gyrotrons, and two additional gyrotrons are in the procurement phase. Each gyrotron experiences a frequency chirp that lasts up to 500 ms. The final frequency depends on

the temperature of the resonant cavity and hence on the power of emitted microwaves. The CTS receiver picks up stray radiation from all gyrotrons due to the layout of the diagnostic. Therefore the receiver has to be adequately protected by broad and deep notch filters.
In addition, the operation of the diagnostic at the heating gyrotron frequency implies the presence of strong electron cyclotron emission background in the keV range for the bean-shaped cross-section and several hundred eV in the triangular cross-section [1]. This affects the signal-to-noise ratio SNR of the CTS measurements, which is given by the following expression:

$$SNR = \frac{P_s\sqrt{Wt}}{\sqrt{2(P_s + P_b)^2 + 2P_b^2}}, \tag{2.1}$$

where P_s is the spectral power density of the scattering signal, W is the frequency bandwidth of a receiver channel, t is the total integration time, and P_b is the spectral power density of the background.
The diagnostic performance at 140 GHz is sufficient for the proof-of-principle measurements of ion temperature in typical low and medium performance plasmas of Wendelstein 7-X. In such plasmas the receiver should be able working in future campaigns as well, since 140 GHz probing radiation causes fewest problems to the other machine systems from the stray radiation. However, at that frequency, refraction significantly influences the beam paths of both probe and receiving beams in the triangular cross-section. Refraction is substantially reduced for 175 GHz as shown in the next section.

3 Upgrade to a higher frequency

Vacuum-air interfaces present difficulties associated with transmitting microwave power to the plasma. Two such interfaces must be passed: one from the gyrotron to the transmission line and the other from the transmission line into the vacuum vessel. The problem is that the vacuum window should absorb only very small fraction of the transmitted power and have extremely good thermal conductivity. As a result only a synthetic diamond window is an option. The reflections from the interface should also be suppressed, which limits the thickness of the window to a multiple of half-wavelengths. The diamond windows at W7-X are optimized for harmonics of 35 GHz, leaving 105 and 175 GHz as possible options close to 140 GHz.

Generally, moving away from 140 GHz either to higher or lower frequencies would significantly reduce the electron cyclotron emission background. At 105 GHz, the scattering cross-section is also typically higher than at 175 GHz. However, a low probing frequency also implies a low cut-off density in the plasma, and the resulting strong refraction then becomes a showstopper, especially for the triangular cross-section. The problem with the triangular cross-section is that the receiving antenna launches fairly tangentially and its steering capabilities are limited. The receiving antenna accepts broadband radiation and can be steered in 1D, but the launcher is a remote steering rectangular corrugated waveguide which is optimized for 140 GHz only [32]. Thus, there is only one launching direction possible for any other probing frequency, which makes finding the overlap between the probe and the scattering beams a real challenge in the case of refraction. This problem is illustrated

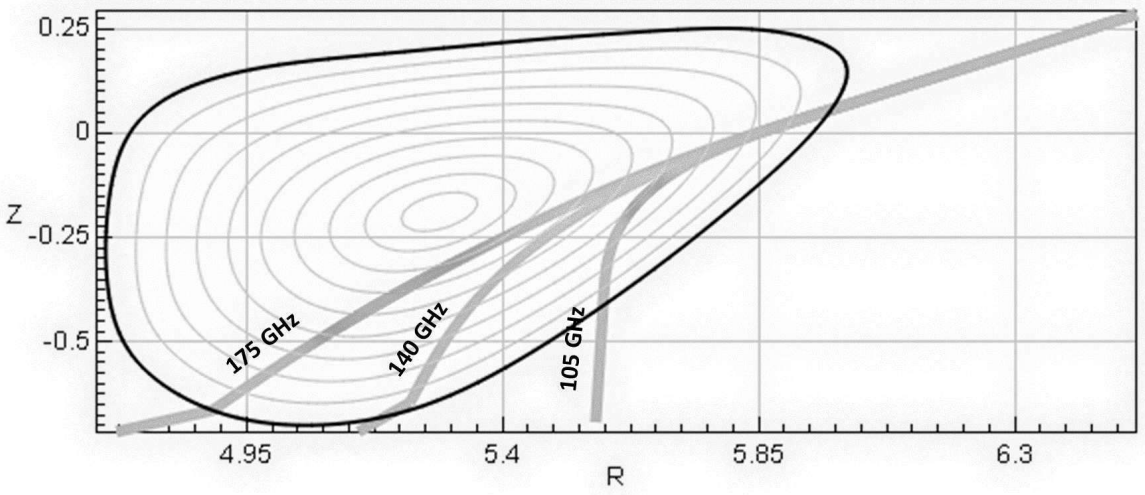

Figure 1. Three beams in O-mode polarization at 175 GHz, 140 GHz, and 105 GHz traced from the reference position of the CTS antenna in the triangular cross-section using the TRAVIS ray-tracing code. Plasma parameters in the center: $n_e = 10^{20}\ m^{-3}$, $T_e = 3$ keV.

in Fig. 1, where three beams originating at the reference position of the CTS receiving antenna in the triangular cross-section are traced. The beams are launched in ordinary mode (O-mode) at 105 GHz, 140 GHz, and 175 GHz into the plasma. The central electron density of $n_e = 10^{20}\ m^{-3}$, and the central electron temperature of $T_e = 3$ keV. The tracing is done by the beam-tracing code TRAVIS [33]. One sees that the 105 GHz beam refracts very strongly. For higher frequencies the beams are gradually refracted less, making 175 GHz a more attractive option than 105 GHz. For this reason, 175 GHz is the frequency of choice for the upgraded CTS system.

It was shown theoretically that the current probing gyrotron is able to emit at the frequency of 173.92 GHz using a $TE_{34,10}$ cavity mode instead of the current $TE_{28,8}$ cavity mode. For this mode less than 5% of the microwave power is converted into stray radiation. The output power will be at the level of 60% of the output power at 140 GHz, and new phase-correcting mirrors will be necessary. A stronger magnet for the gyrotron that generates up to 7 T will be procured. At 175 GHz, the high frequency probing beam in the triangular cross-section will not be absorbed by the plasma and will be terminated by a beam dump after the first pass. At the bean-shaped cross-section a beam dump is not foreseen.
The CTS receiver will be equipped with a new horn antenna that is capable of working in both 140 GHz and 175 GHz frequency ranges and a new high frequency back-end for the new frequency range. The intermediate frequency part of the receiver, as well as the data acquisition system will be retained. For the details of the current CTS receiver see reference [1].

3.1 Collective Thomson scattering spectra due to thermal ions

The main task of the current and upgraded CTS system is ion temperature measurements. To evaluate the performance of the upgraded diagnostic at 175 GHz, we computed the associated CTS spectrum

due to thermal ions, assuming scattering from O-mode to O-mode and from the extraordinary mode (X-mode) to X-mode for both the triangular and bean-shaped cross-sections, see Fig. 2(a). We assumed a hydrogen plasma with 1.5% carbon content and the following parameters: electron temperature T_e = 2.3 keV, electron density $n_e = 6 \cdot 10^{19}$ m^{-3}, ion temperature T_i = 2 keV, power of the probing beam P_{probe} = 400 kW, overlap integral (normalized volume integral of the product of intensities of the probing and receiver beams) O_b = 30 m^{-1}. The difference between X-mode to X-mode scattering (red lines) and O-mode to O-mode (blue lines) scattering is explained by higher scattering cross-section in the X to X mode scattering channel in comparison to the O to O mode scattering channel. The difference in the spectral width for the triangular cross-section (solid lines) and bean-shaped cross-section (dashed lines) is explained by the scattering geometry. The width of the spectrum is proportional to the length of $\vec{k^\delta} = \vec{k^s} - \vec{k^i}$, where $\vec{k^s}$ and $\vec{k^i}$ represent the wave vectors of scattering and incident waves, respectively. In the triangular cross-section $\vec{k^i}$ and $\vec{k^s}$ are nearly perpendicular to each other, and the scattering angle is $\theta = \angle(\vec{k^i}, \vec{k^s}) = 95°$. In contrast, in the bean-shaped cross-section the scattering angle is θ=160°, which is nearly a backscattering geometry. This results in a larger length of $\vec{k^\delta}$ and hence a broader spectrum at the same temperature. The difference in in normalization between spectra from the different cross-sections is primarily due to differences in polar angle ψ of the projection of the magnetic field onto the plane that has the x-axis aligned with $\vec{k^i} \times \vec{k^s}$ and the y-axis aligned with $\vec{k^\delta} \times (\vec{k^i} \times \vec{k^s})$. For the triangular cross-section ψ = 28° and for the bean-shaped cross-section ψ = 350°.

For ion temperature inference a signal-to-noise ratio of at least 10 is desirable. Fig. 2(b) shows predicted integration times as a function of the spectral power density of the background for a frequency channel with 20 MHz bandwidth at the frequency 1.5 GHz away from the probe frequency in the bean-shaped cross-section and 1.13 GHz away from the probe frequency in the triangular cross-section. Thus different spectral widths in the different cross-sections are taken into account. The frequency shifts are limiting the thermal spectra in the bean-shaped and triangular cross-sections, respectively, and the bandwidth is typical for the thermal spectra analysis. The signal in these bands has lowest spectral power density and allow conservative estimations of the integration time. Average spectral power densities are: 340 meV (O-O scattering, triangular cross-section), 560 meV (X-X scattering, triangular cross-section), 640 meV (O-O scattering, bean-shaped cross-section), and 1000 meV (X-X scattering, bean-shaped cross-section). TRAVIS predicts zero electron cyclotron emission background for the standard magnetic configuration with the on-axis magnetic field of 2.52 T at zero toroidal angle (typical magnetic configuration for W7-X). However, the first measurements with the Michelson interferometer [34] in the last experimental campaign showed a weak signal in the frequency range of interest. The signal was uncalibrated but is estimated to lie in the order of several eV. The nature of this weak signal may be due to the hardware but bremsstrahlung from the plasma cannot be excluded. However, even in the case of 10 eV background, the integration time required for achieving signal-to-noise ratio of 10 will not exceed 20 ms for the triangular cross-section, which is smaller than the hardware limits of the receiver.

3.2 Collective Thomson scattering spectra due to fast ions

Two neutral beam injection (NBI) sources were commissioned at W7-X in the first divertor campaign [35]. Two more sources will be added in the next campaign with a water-cooled divertor. Ion cyclotron heating will also be commissioned in the next campaign [36] for ion heating and fast ion

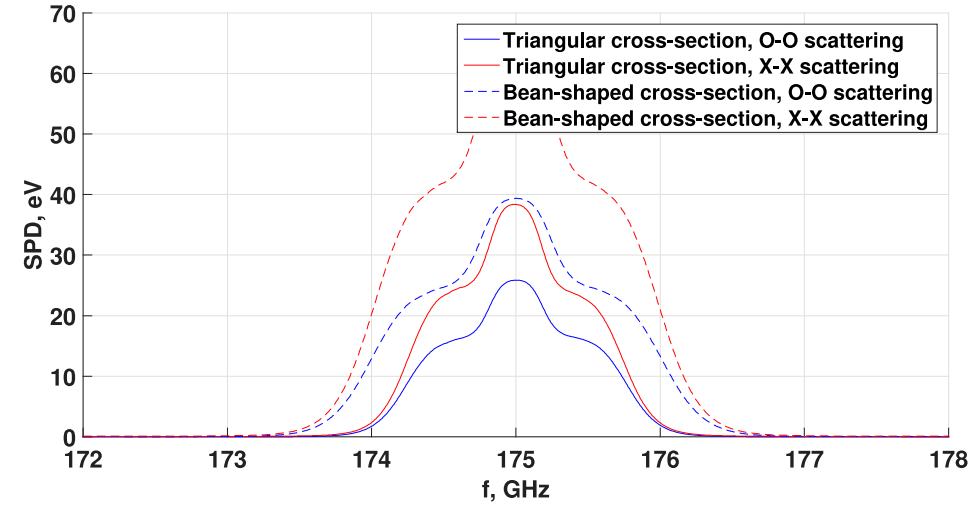

(a)

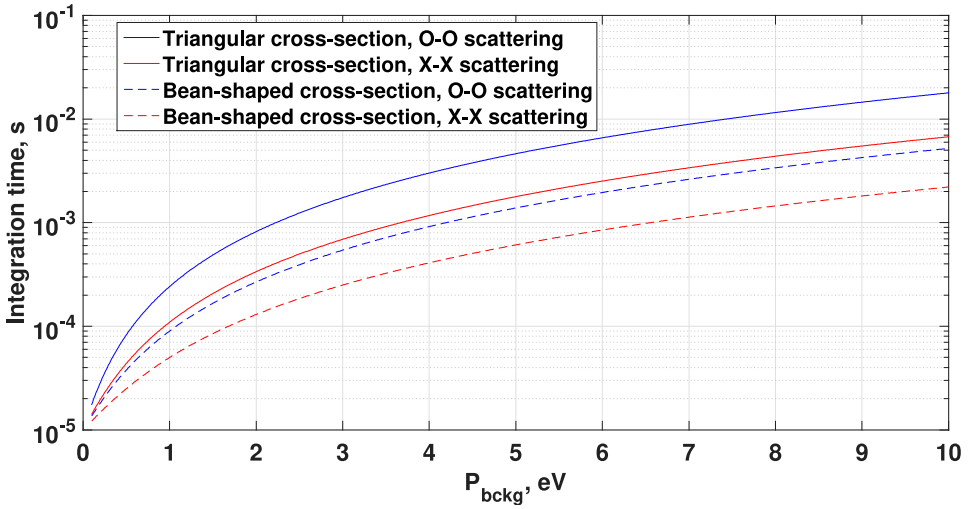

(b)

Figure 2. (a) Predicted spectral power density (SPD) of the thermal spectrum for a hydrogen plasma with 1.5% carbon. Simulation parameters: scattering angle $\theta = 95°$ for the triangular cross-section and $\theta = 160°$ for the bean-shaped one, angle of the resolved fluctuations to the magnetic field $\phi = \angle(\vec{B}, \vec{k^{\delta}}) = 80°$ in both cases, $\psi = 28°$ for the triangular and $\psi = 350°$ for the bean-shaped cross-sections, magnetic field B=2.3 T for the triangular cross-section and B=2.5 T for the bean-shaped cross-section, electron density $n_e = 6 \cdot 10^{19}$ m^{-3}, ion temperature $T_i = 2$ keV, electron temperature $T_e = 2.3$ keV, overlap integral $O_b = 30$ m^{-1}, power of the probing beam $P_{probe} = 400$ kW. The spectra for the triangular cross-section are plotted as solid lines and for the bean-shaped cross-section as dashed lines; the spectra for the O-O scattering are plotted in blue and for X-X scattering in red. (b) Integration time for achieving signal-to-noise ratio=10 as a function of the spectral power density of the background for a frequency channel with 20 MHz bandwidth at the frequency 1.5 GHz away from the probe frequency in the bean-shaped cross-section and 1.13 GHz away from the probe frequency in the triangular cross-section.

generation [37, 38].
CTS measurements are sensitive to $g(u)$, the fast-ion velocity distribution projected onto $\vec{k}^{\delta}$.To assess the prospects for CTS fast-ion measurements at 175 GHz in W7-X, the fast-ion velocity distribution function from two hydrogen NBI sources with a total power of 2.9 MW and beam energy of 50 keV was modelled using ASCOT [39]. Assumed plasma and scattering parameters remain the same as in Section 3.1. The projected fast ion velocity distribution function in the center of the triangular cross-section is shown in Fig. 3(a). The resulting contribution of fast ions to the scattering spectrum is defined as the difference in spectral power density between spectra simulated with and without fast ions for the same thermal-ion plasma parameters. The corresponding contribution of fast ions to the scattering spectrum is shown in Fig. 3(b). The same projection of the fast ion velocity distribution function is used to simulate the spectra, although higher fast ion densities are expected in the bean-shaped cross-section in comparison to the triangular cross-section because a magnetic field well is located in the triangular cross-section.

Fig. 4 shows predicted integration times required to reach a signal-to-noise ratio of 10 within a frequency channel with 200 MHz bandwidth at a central frequency of 177 GHz for the triangular cross-section and at 177.7 GHz for the bean-shaped cross-section. The results show that the integration time must exceed 1 s for O-O scattering in the triangular cross-section at a background spectral power density of 10 eV. The integration time for the same background drops to 250 ms in the case of X-X scattering in the bean-shaped cross-section. The total integration time is limited by the memory of the fast digitizer of the receiver (1 GB). It can sample approximately 170 ms of continuous data. It implies that for achieving the target value of signal-to-noise ratio of ten, maximum background level should not exceed 4 eV for the triangular cross-section and 5.5 eV for the bean-shaped cross-section. In the case of high background, the measurements will have to be performed with lower signal-to-noise ratio or with coarser frequency binning.

4 Conclusions

The existing CTS diagnostic at Wendelstein 7-X operates using a 140 GHz heating gyrotron as the source of probing radiation, and proof-of-principle measurements with this setup have been successfully conducted. Nevertheless, we have here highlighted the need to transition to a higher frequency, in order to improve the signal-to-noise ratio of the diagnostic and reduce the impact of refraction, which is significant at typical electron densities in Wendelstein 7-X. With some modifications, the present Wendelstein 7-X gyrotrons are capable of emitting at a frequency of 173.92 GHz with limited stray radiation in the gyrotron itself. At this frequency, the diamond windows in the gyrotron tramission lines retain their non-reflective properties, and background electron cyclotron emission from the plasma is minimized. To evaluate the diagnostic performance at frequencies around 175 GHz, we computed resulting thermal and fast ion-induced scattering spectra for typical Wendelstein 7-X plasma parameters. These spectra show that it is possible to obtain high quality scattering spectra for ion temperature measurements (signal-to-noise ratio of 10) across a wide range of background levels. However, fast-ion measurements with signal-to-noise ratio greater than 10 are only achievable in the case of very low background: less than 4 eV for the triangular cross-section and less than 5.5 eV for the bean-shaped cross-section.

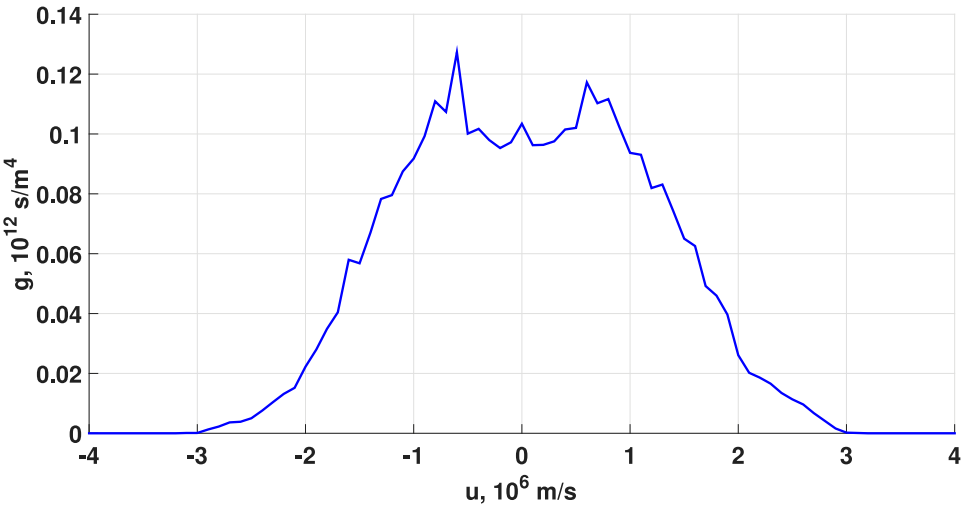

(a)

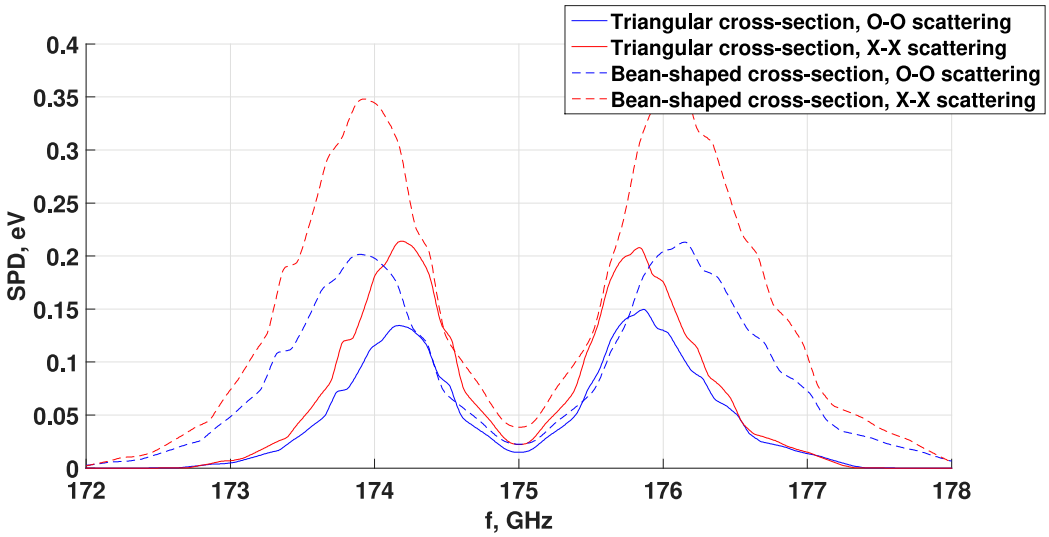

(b)

Figure 3. (a) Projection of the fast-ion velocity distribution function $g(u)$ in the center of the triangular cross-section of W7-X, assuming P_{NBI} = 2.9 MW and an injection energy of the beam particles of 50 keV.; (b) Simulated contribution of fast ions to the scattering spectrum using the scattering parameters as in Section 3.1. The spectra for the triangular cross-section are plotted as solid lines and for the bean-shaped cross-section as dashed lines; the spectra for O-O scattering are plotted in blue and for X-X scattering in red.

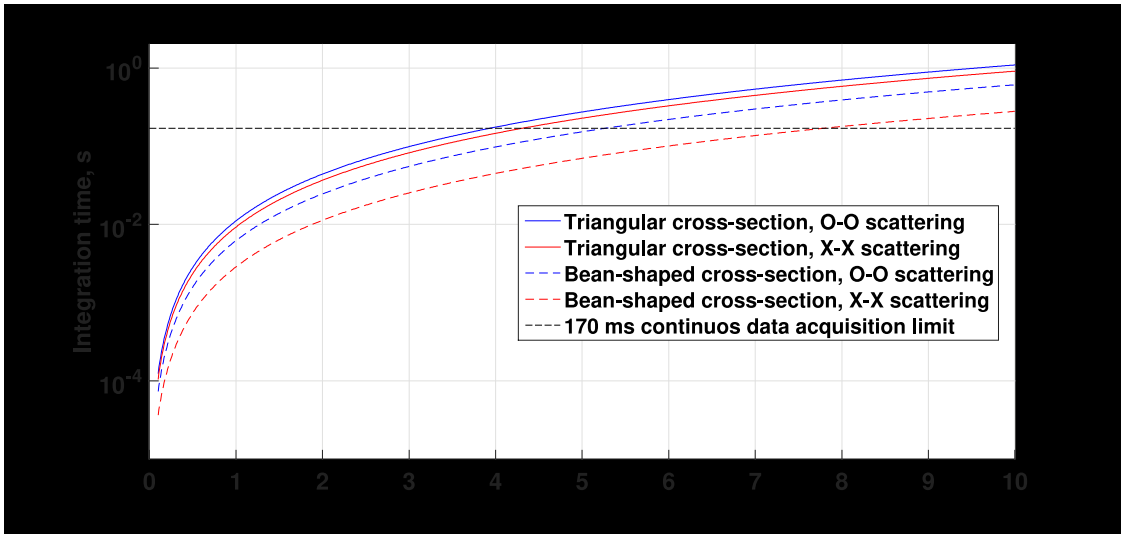

Figure 4. Predicted integration time for achieving a signal-to-noise ratio of 10 as a function of the spectral power density of the background for a frequency channel with 200 MHz bandwidth at the frequency 2.66 GHz away from the probe frequency in the bean-shaped cross-section and 2 GHz away from the probe frequency in the triangular cross-section. The predictions for the triangular cross-section are plotted as solid lines and for the bean-shaped cross-section as dashed lines; the predictions for the O-O scattering channel are plotted in blue and for the X-X scattering channel in red.

Acknowledgments

This work has been carried out within the framework of the EUROfusion Consortium and has received funding from the Euratom research and training program 2014–2018 and 2019–2020 under grant agreement No. 633053. The views and opinions expressed herein do not necessarily reflect those of the European Commision.

References

[1] D. Moseev, M. Stejner, T. Stange, I. Abramovic, H. P. Laqua, S. Marsen et al., *Collective Thomson scattering diagnostic at Wendelstein 7-X*, *Review of Scientific Instruments* **90** (jan, 2019) 013503.

[2] I. Abramovic, A. Pavone, D. Moseev, N. J. Lopes Cardozo, M. Salewski, H. P. Laqua et al., *Forward modeling of collective Thomson scattering for Wendelstein 7-X plasmas: Electrostatic approximation*, *Review of Scientific Instruments* **90** (feb, 2019) 023501.

[3] J. Svensson, O. Ford, D. McDonald, A. Meakins, A. Werner, M. Brix et al., *Modelling of JET Diagnostics Using Bayesian Graphical Models*, *Contributions to Plasma Physics* **51** (mar, 2011) 152–157.

[4] I. Abramovic, M. Salewski and D. Moseev, *Collective Thomson scattering model for arbitrarily drifting bi-Maxwellian velocity distributions*, *AIP Advances* **9** (mar, 2019) 035252.

[5] M. Stejner, J. Rasmussen, S. K. Nielsen, A. S. Jacobsen, S. B. Korsholm, F. Leipold et al., *Main-ion temperature and plasma rotation measurements based on scattering of electron cyclotron heating waves in ASDEX Upgrade*, *Plasma Physics and Controlled Fusion* **59** (jul, 2017) 075009.

[6] S. B. Korsholm, M. Stejner, H. Bindslev, V. Furtula, F. Leipold, F. Meo et al., *Measurements of Intrinsic Ion Bernstein Waves in a Tokamak by Collective Thomson Scattering*, *Phys. Rev. Lett.* **106** (apr, 2011) 165004.

[7] M. Stejner, M. Salewski, S. B. Korsholm, H. Bindslev, E. Delabie, F. Leipold et al., *Measurements of ion temperature and plasma hydrogenic composition by collective Thomson scattering in neutral beam heated discharges at TEXTOR*, *Plasma Physics and Controlled Fusion* **55** (aug, 2013) 085002.

[8] M. Stejner, S. K. Nielsen, H. Bindslev, S. B. Korsholm and M. Salewski, *Principles of fuel ion ratio measurements in fusion plasmas by collective Thomson scattering*, *Plasma Physics and Controlled Fusion* **53** (jun, 2011) 065020.

[9] M. Stejner, S. B. Korsholm, S. K. Nielsen, M. Salewski, H. Bindslev, S. Brezinsek et al., *Measurements of plasma composition in the TEXTOR tokamak by collective Thomson scattering*, *Plasma Physics and Controlled Fusion* **54** (jan, 2012) 015008.

[10] M. Stejner, S. K. Nielsen, A. S. Jacobsen, S. B. Korsholm, F. Leipold, R. M. McDermott et al., *Plasma rotation and ion temperature measurements by collective Thomson scattering at ASDEX Upgrade*, *Plasma Physics and Controlled Fusion* **57** (jun, 2015) 062001.

[11] M. Stejner, S. B. Korsholm, S. K. Nielsen, M. Salewski, H. Bindslev, F. Leipold et al., *Temporally resolved plasma composition measurements by collective Thomson scattering in TEXTOR (invited).*, *The Review of scientific instruments* **83** (oct, 2012) 10E307.

[12] S. K. Nielsen, M. Stejner, J. Rasmussen, A. S. Jacobsen, S. B. Korsholm, F. Leipold et al., *Measurements of the fast-ion distribution function at ASDEX upgrade by collective Thomson scattering (CTS) using active and passive views*, *Plasma Physics and Controlled Fusion* **57** (mar, 2015) 035009.

[13] S. K. Nielsen, H. Bindslev, M. Salewski, A. Bürger, E. Delabie, V. Furtula et al., *Fast-ion redistribution due to sawtooth crash in the TEXTOR tokamak measured by collective Thomson scattering*, *Plasma Physics and Controlled Fusion* **52** (sep, 2010) 092001.

[14] D. Moseev, F. Meo, S. B. Korsholm, T. Koskela, M. Albergante, O. Asunta et al., *Comparison of measured and simulated fast ion velocity distributions in the TEXTOR tokamak*, *Plasma Physics and Controlled Fusion* **53** (2011) 105004.

[15] J. Rasmussen, S. K. Nielsen, M. Stejner, B. Geiger, M. Salewski, A. S. Jacobsen et al., *Consistency between real and synthetic fast-ion measurements at ASDEX Upgrade*, *Plasma Physics and Controlled Fusion* **57** (jul, 2015) 075014.

[16] M. Salewski, F. Meo, M. Stejner, O. Asunta, H. Bindslev, V. Furtula et al., *Comparison of fast ion collective Thomson scattering measurements at ASDEX Upgrade with numerical simulations*, *Nuclear Fusion* **50** (mar, 2010) 035012.

[17] S. K. Nielsen, M. Salewski, H. Bindslev, A. Bürger, V. Furtula, M. Kantor et al., *Dynamics of fast ions during sawtooth oscillations in the TEXTOR tokamak measured by collective Thomson scattering*, *Nuclear Fusion* **51** (2011) 063014.

[18] M. Nishiura, S. Kubo, K. Tanaka, N. Tamura, T. Shimozuma, T. Mutoh et al., *Initial result of collective Thomson scattering using 77 GHz gyrotron for bulk and tail ion diagnostics in the Large Helical Device*, *Journal of Physics: Conference Series* **227** (may, 2010) 012014.

[19] M. Nishiura, S. Kubo, K. Tanaka, R. Seki, S. Ogasawara, T. Shimozuma et al., *Spectrum response and analysis of 77 GHz band collective Thomson scattering diagnostic for bulk and fast ions in LHD plasmas*, *Nuclear Fusion* **54** (feb, 2014) 023006.

[20] S. Kubo, M. Nishiura, K. Tanaka, T. Shimozuma, Y. Yoshimura, H. Igami et al., *Collective Thomson scattering of a high power electron cyclotron resonance heating beam in LHD (invited).*, *The Review of scientific instruments* **81** (oct, 2010) 10D535.

[21] A. G. Shalashov, E. V. Suvorov, L. V. Lubyako and H. Maassberg, *NBI-driven ion cyclotron instabilities at the W7-AS stellarator*, *Plasma Physics and Controlled Fusion* **45** (apr, 2003) 395–412.

[22] M. Salewski, B. Geiger, W. W. Heidbrink, A. S. Jacobsen, S. B. Korsholm, F. Leipold et al., *Doppler tomography in fusion plasmas and astrophysics*, *Plasma Physics and Controlled Fusion* **57** (jan, 2015) 014021.

[23] M. Salewski, B. Geiger, S. Nielsen, H. Bindslev, M. García-Muñoz, W. Heidbrink et al., *Combination of fast-ion diagnostics in velocity-space tomographies*, *Nuclear Fusion* **53** (jun, 2013) 063019.

[24] M. Salewski, B. Geiger, A. Jacobsen, M. García-Muñoz, W. Heidbrink, S. Korsholm et al., *Measurement of a 2D fast-ion velocity distribution function by tomographic inversion of fast-ion D-alpha spectra*, *Nuclear Fusion* **54** (feb, 2014) 023005.

[25] M. Salewski, S. Nielsen, H. Bindslev, V. Furtula, N. Gorelenkov, S. Korsholm et al., *On velocity space interrogation regions of fast-ion collective Thomson scattering at ITER*, *Nuclear Fusion* **51** (aug, 2011) 083014.

[26] M. Salewski, B. Geiger, S. Nielsen, H. Bindslev, M. García-Muñoz, W. Heidbrink et al., *Tomography of fast-ion velocity-space distributions from synthetic CTS and FIDA measurements*, *Nuclear Fusion* **52** (oct, 2012) 103008.

[27] D. Moseev, M. Salewski, M. Garcia-Muñoz, B. Geiger and M. Nocente, *Recent progress in fast-ion diagnostics for magnetically confined plasmas*, *Reviews of Modern Plasma Physics* **2** (dec, 2018) 7.

[28] V. Erckmann, P. Brand, H. Braune, G. Dammertz, G. Gantenbein, W. Kasparek et al., *The 140 GHz, 10 MW, CW ECRH Plant for W7-X: A Training Field for ITER*, in *Fusion Energy 2006*, (Chengdu), pp. IT/2–4Rd, International Atomic Energy Agency, 2007.

[29] V. Erckmann, P. Brand, H. Braune, G. Dammertz, G. Gantenbein, W. Kasparek et al., *Electron Cyclotron Heating for W7-X: Physics and Technology*, *Fusion Science and Technology* **52** (aug, 2007) 291–312.

[30] G. Michel, V. Erckmann, F. Hollmann, L. Jonitz, W. Kasparek, H. Laqua et al., *Matching of the ECRH transmission line of W7-X*, *Fusion Engineering and Design* **88** (oct, 2013) 903–907.

[31] R. C. Wolf, S. Bozhenkov, A. Dinklage, G. Fuchert, Y. O. Kazakov, H. P. Laqua et al., *Electron-cyclotron-resonance heating in Wendelstein 7-X: A versatile heating and current-drive method and a tool for in-depth physics studies*, *Plasma Physics and Controlled Fusion* **61** (jan, 2019) 014037.

[32] B. Plaum, G. Gantenbein, W. Kasparek, K. Schwörer, M. Grünert, H. Braune et al., *High-Power Tests of a Remote-Steering Antenna at 140 GHz*, *Fusion Engineering and Design* **50** (2017) 1–14.

[33] N. Marushchenko, Y. Turkin and H. Maassberg, *Ray-tracing code TRAVIS for ECR heating, EC current drive and ECE diagnostic*, *Computer Physics Communications* **185** (jan, 2014) 165–176.

[34] J. W. Oosterbeek, N. Chaudhary, M. Hirsch, U. Höfel and R. C. Wolf, *Assessment of ECH stray radiation levels at the W7-X Michelson Interferometer and Profile Reflectometer*, *EPJ Web of Conferences* **203** (mar, 2019) 03010.

[35] R. C. Wolf, A. Alonso, S. Äkäslompolo, J. Baldzuhn, M. Beurskens, C. D. Beidler et al., *Performance of Wendelstein 7-X stellarator plasmas during the first divertor operation phase*, *Physics of Plasmas* **26** (aug, 2019) 082504.

[36] B. Schweer, J. Ongena, V. Borsuk, D. Birus, S. Bozhenkov, D. C. Bardawil et al., *Development of an ICRH antenna system at W7-X for plasma heating and wall conditioning*, *Fusion Engineering and Design* **123** (nov, 2017) 303–308.

[37] Y. O. Kazakov, J. Ongena, J. C. Wright, S. J. Wukitch, E. Lerche, M. J. Mantsinen et al., *Efficient generation of energetic ions in multi-ion plasmas by radio-frequency heating*, *Nature Physics* **13** (oct, 2017) 973–978.

[38] J. M. Faustin, J. P. Graves, W. A. Cooper, S. Lanthaler, L. Villard, D. Pfefferlé et al., *Modelling of advanced three-ion ICRF heating and fast ion generation scheme for tokamaks and stellarators*, *Plasma Physics and Controlled Fusion* **59** (aug, 2017) 084001.

[39] S. Äkäslompolo, M. Drevlak, Y. Turkin, S. Bozhenkov, T. Jesche, J. Kontula et al., *Modelling of NBI ion wall loads in the W7-X stellarator*, *Nuclear Fusion* **58** (aug, 2018) 082010.